Available online at www.sciencedirect.com
ScienceDirect
C. R. Mecanique 337 (2009) 693–702
COMPTES RENDUS MECANIQUE

Cuspidal caustic and focusing of acoustical waves generated by a parametric array onto a concave reflecting surface

Bernard Castagnède *, Sohbi Sahraoui, Vincent Tournat, Najat Tahani

Laboratoire d'acoustique, UMR CNRS 6613, université du Maine, avenue Olivier-Messiaen, 72085 Le Mans cedex 9, France

Received 22 May 2009; accepted after revision 8 September 2009

Available online 30 September 2009

Presented by Jean-Baptiste Leblond

Abstract

The present Note is devoted to the study of the so-called cuspidal caustic at the surface of a hemi-cylindrical reflector illuminated with plane waves. In order to generate low frequency (e.g. in the range of 4 kHz) acoustical plane waves, a commercially available parametric array has been used. It produces powerful ultrasonic carrier waves at 40 kHz which can be electronically modulated between 200 Hz and 10 kHz. Further self-demodulation process during propagation in air generates an ultra-directive acoustical field (i.e. quasi-planar wavefronts) enabling to accurately study the focusing process occurring along the cuspidal caustic. The focusing coefficient can be computed locally by using two numerical tools, on one hand by computing the density of tangent rays to the caustic, and on the other hand by using some numerical results provided by a ray tracing algorithm. Some preliminary experimental data are then provided in order to validate the numerical predictions (spatial position of the caustic and focusing coefficient). ***To cite this article: B. Castagnède et al., C. R. Mecanique 337 (2009).***
© 2009 Published by Elsevier Masson SAS on behalf of Académie des sciences.

Résumé

Caustique en « corne de croissant » et focalisation des ondes acoustiques générées par une antenne paramétrique. Ce travail est consacré à l'étude de la caustique en « corne de croissant » à la surface d'un réflecteur hémi-cylindrique illuminée par des ondes planes. En vue de générer des ondes planes acoustiques de basse fréquence (autour de 4 kHz), une antenne paramétrique disponible commercialement a été utilisée. Elle produit une onde ultrasonore porteuse de forte puissance à 40 kHz qui peut-être modulée en amplitude de façon électronique entre 200 Hz et 10 kHz. Le processus d'auto-démodulation au cours de la propagation dans l'air permet de générer un champ acoustique ultra-directif (c'est-à-dire des ondes quasi-planes) autorisant une étude précise de la focalisation le long de la caustique. Le coefficient de focalisation est alors calculé localement, en utilisant deux approches numériques différentes, d'une part en calculant la densité de rayons tangents à la caustique et d'autre part en mettant en œuvre une méthode de calcul du type tracé de rayons. Des résultats expérimentaux préliminaires sont alors décrits avec l'objectif de valider les prédictions numériques (position spatiale de la singularité et coefficient de focalisation). ***Pour citer cet article : B. Castagnède et al., C. R. Mecanique 337 (2009).***
© 2009 Published by Elsevier Masson SAS on behalf of Académie des sciences.

Keywords: Acoustics; Low frequency propagation onto an half-cylindrical reflector; Cuspidal caustic; Focusing coefficient; Nonlinear acoustic parametric array; Ray tracing algorithm

* Corresponding author.
E-mail address: bernard.castagnede@univ-lemans.fr (B. Castagnède).

1631-0721/$ – see front matter © 2009 Published by Elsevier Masson SAS on behalf of Académie des sciences.
doi:10.1016/j.crme.2009.09.006

Mots-clés : Acoustique ; Propagation sur un réflecteur hémi-cylindrique ; Caustique en corne de croissant ; Coefficient de focalisation ; Calcul du type tracé de rayons

1. Introduction and position of the problem

Caustics and focusing are two concepts which are inherently linked together. They are related to some inhomogeneity occurring within a propagation process, having very diverse origins. For instance, in solid state physics, anisotropy is responsible for phonon focusing at the same time for volume and surface ultrasonic waves [1–5]. In fact, the phonon focusing effect is the consequence of the wave energy direction which is orthogonal to the phase slowness curves (i.e. the polar plot of the inverse of the phase wavespeed, or 3D slowness surface sheets when propagation is seen in the full 3D environment). Due to the intricacies of the 3D principal curvatures of the associated slowness sheets of the bulk, shear and 2D surface waves inside anisotropic crystals (or at their interfaces), wonderful effects and images can be found in the literature. Similar effects exist as well in underwater acoustics, and for long range propagation in inhomogeneous media [6–10]. Here the focusing effects are explained by gradient properties within the propagating media creating channelling multi-layered structures, or they are due to subtle inhomogeneity effects for long range propagation, in some cases linked to mirage behaviour in moving media, and so forth. Caustics and focusing effects have also been studied when nonlinear acoustic behaviour are considered, as well as in water [11], and in air propagation such as for the propagation of shock waves during sonic boom [12–14]. Turbulent flows are also at the origin of focusing effects and at the onset of caustics, as it was clearly established during the last 20 years [15–18]. This even constitutes a potential powerful tool to characterise turbulence through adequate descriptors. In the field of applied mechanics, optical methods have been widely used to characterise engineering materials (e.g. see [19] for an application of optical engineering to evaluate stress concentrations in materials) and numerous papers were written in that area. Another field of study and applications is related to granular materials for which gravity produces vertical gradients of the physical properties, resulting in the possibility to observe focusing during propagation along an horizontal axis [20–22].

Caustics and focusing effects are then spatio-temporal singularities occurring during propagation in anisotropic, inhomogeneous, moving and turbulent media. These effects can be described by catastrophe theory, by specialised singular mathematical treatments and ad-hoc theoretical tools [23–28]. Most of these features are inherently related to the transient fields and to causality principles. In air duct acoustics, some effects have been studied, for instance in the field of aeronautics and applied acoustics [29,30]. On the other hand, it is well known that boundary effects might also produce focusing effects and sound concentration. In some cases, for instance, during propagation along ducts one might observe focusing effects and caustics as well [31,32]. Such effects are at the base of acoustic field transformations. An other example is related to a plane wave insonifying an elliptical reflector that will focus at its *well-named* focus point. Normally, a plane wave impinging a cylindrical reflector should produce cylindrical waves somehow converging towards its central axis, but the reality is a little bit more subtle. This is precisely such geometry which has been studied in the present paper. In fact, plane waves are focusing onto a cuspidal caustic having a particular shape. This is a very well-known problem of physical acoustics (for instance see [33] for a review by Philip L. Marston, or [34] for a reference text book), that has been here somewhat revisited with proper numerical and experimental tools. This configuration is first studied analytically in the next section, then numerically by using simple geometrical ray simulations as well as with an appropriate ray tracing algorithm. The main novelty of this paper deals with the experimental data obtained in the audio range in air, which uses a special device producing planar acoustical wavefronts at low frequency. This set-up consists in using a commercially available parametric array enabling producing quasi-plane waves over the 200 Hz–10 kHz acoustical bandwidth. The paper is then ended by concluding remarks and a prospective discussion.

2. Basic features of the cuspidal caustic of a half-cylindrical reflector

Fig. 1 provides the basic geometry pertaining to the case of the reflection of a planar acoustical wavefront (also called eikonal function) onto a quarter (or by extension, due to symmetry, to a half) cylindrical reflector. Similar results and analysis could easily be extended to other geometries, such as spherical, parabolic, elliptical half reflectors. Specifically, Fig. 1 shows an incident ray impinging the shell at point M having polar coordinates $(R\cos\theta,\ R\sin\theta)$,

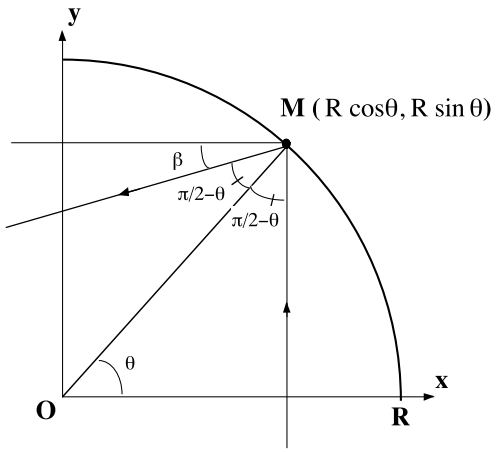

Fig. 1. Geometry of the problem and definitions of the modelling parameters.

where R represents the inner radius of the cylindrical reflector, and θ the angle with respect to the horizontal axis Ox. Next, the incident ray is specularly reflected back by the cylindrical surface which acts as a perfect reflector. By direct inspection, the angle β of Fig. 1 is linked to θ, as given by the straightforward relationship $\beta = 2\theta - \pi/2$. The specularly reflected wave is then described by the trivial equation of a straight line, $y = ax + b$, where a is simply provided by direct inspection as the slope of the line:

$$a = \tan\beta = \tan\left(2\theta - \frac{\pi}{2}\right) = -\frac{1}{\tan 2\theta}$$

Next, the coefficient b is evaluated, just by taking into account that location M belongs to that very same straight line. It follows through trivial algebra that

$$b = R\sin\theta + \frac{R\cos\theta}{\tan 2\theta}$$

Accordingly, the equation of the reflected straight path is then given by the following expression:

$$f(x, y, \theta) = y + \frac{x}{\tan 2\theta} - R\left(\sin\theta + \frac{\cos\theta}{\tan 2\theta}\right) = 0 \tag{1}$$

The cuspidal caustic is just the geometric envelope of the reflected straight paths, and consequently its analytical expression should fulfil the partial derivative over θ of the above expression to be zero. This condition finally yields the following equation:

$$f'(x, y, \theta) = 0 \Rightarrow x = \frac{R}{2}\left(\frac{\sin 4\theta}{2}\sin\theta + \cos\theta\left(2 - \sin^2 2\theta\right)\right) \tag{2}$$

This equation with the corresponding expression of $y(\theta)$, as already noted in Eq. (1) provides the parametric analytical equation of the cuspidal caustic for this geometry. Next, one can gain access to the total length of the cuspidal caustic, which by the way is drawn after numerical computations on Fig. 5. For that purpose, one needs to compute the curvilinear integral:

$$\ell = \oint_0^{\frac{\pi}{2}} \sqrt{x'^2 + y'^2}\,\mathrm{d}\theta \tag{3}$$

where x' and y' respectively represents the partial derivative of the cartesian coordinates x and y with respect to θ (as provided by proper derivatives of Eqs. (1) and (2) versus θ). This computation simply provides $\ell = 1.5R$, i.e. 3/2 of the inner radius of the cylindrical shell. This result is also directly observed onto Fig. 5 providing the shape of the cuspidal caustic. At a given initial time providing the initial value of the eikonal function which lies along axis Ox, the ray of order 200 immediately reaches the caustic at point B of Fig. 2, while the reflected ray of order 0 needs to

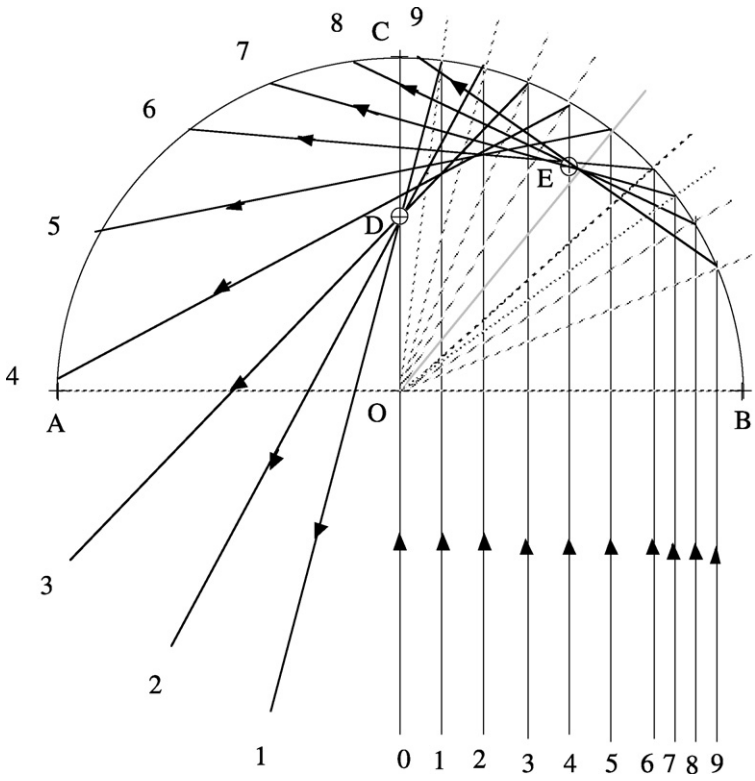

Fig. 2. Schematic ray-tracing illustrating the concept of cuspidal caustic for a quarter cylindrical shell.

propagate until location D of Fig. 2, which simply corresponds to $1.5R$. Alternatively, this last remark indicates that the displacement of the amplitude singularity over the cuspidal caustic is simply done at the speed of sound.

Fig. 2 is a simplified representation of the studied problem showing several rays of the incident plane wavefront. This is obviously a crude representation, but some basic features are already visible in this figure. The focusing process is very seldom at the onset of the very last rays (around location B). Further focusing is definitely present, for instance as drawn at location E or even more pronounced at location D. As a matter of fact, the transition and further increase in the focusing effect is really continuous, and there is no particular reason for having some given intermediate location, such as point E in Fig. 2, which simply is here an artefact of having a denser concentration of incident rays between rays #6 and #9. Evidently, in order to study more precisely the focusing effect, one should use some refined numerical tools. This is exactly what has been done in the next section. A simple ray tracing algorithm has been implemented, enabling to compute precisely the focusing coefficient along the caustic. We have also used a much more simple analysis based on the computation of the density of the tangent reflected waves along the caustic, and both approaches provide very similar results as explained in the following section.

3. Ray tracing algorithm for describing cuspidal caustics

In view to adequately describe the spatio-temporal features of the cuspidal caustic, we have implemented a ray tracing algorithm. It starts with simulating many rays along the initial eikonal planar wavefront (here most often 200 different rays, as documented on most of the figures, but from time to time, up to 20 000 rays have been used). As a matter of fact, at $t = 0$ (initial time), each ray is located along the horizontal axis x, between locations O and B of Fig. 2. Next, we follow the progression of each single ray, at the same time along the incident waves, as well as along the specularly reflected waves when interactions with the inner radius of the half-cylindrical reflector occur. More specifically, we compute the position of the 200 rays, at each $n\Delta t$, where n is between 0 and 200 (or 300 in order to reach location D), and where Δt is the transit time to travel the radius of the reflector divided by 200. Say in other words, the spatial and temporal finite differences are kept the same in order to evaluate the propagation of the

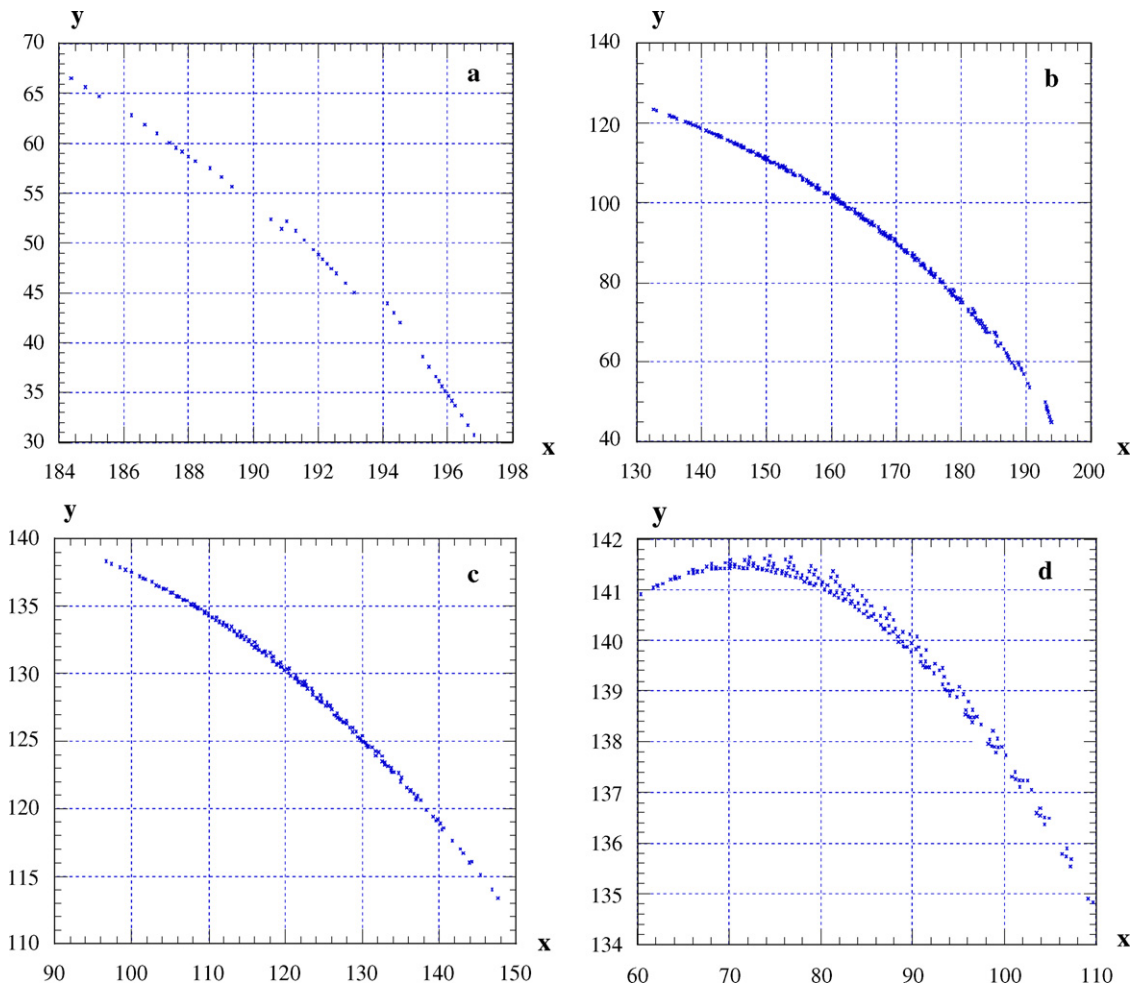

Fig. 3. Results of a ray tracing algorithm showing rays arrivals around the caustic feature. The tracing is done on the 4 various pictures by plotting the progression of only one single ray over two with the following parameters: (a) rays order from 151 to 200; (b) rays order from 101 to 150; (c) rays order from 76 to 100; (d) rays order from 51 to 75.

individual rays with the same resolution at the same time along the spatial coordinate x and for the temporal delays Δt. For instance, in order to describe phenomena until the ray #0 reaches location D, one needs to account for $300\Delta t$, and this number for any of the 200 spatial rays, results in $200 \times 300 = 60\,000$ data points to be computed. Evidently, we do not have to plot all these data, as we generally do concentrate on synchronicity (i.e. two or several different rays arriving at the same time at the same location) of the reflected waves in the vicinity of the caustic. In fact, we only plot the various rays converging at the same time towards the caustic area, even if we cannot totally avoid plotting more data than necessary. Figs. 3 and 4 provide some simple numerical results obtained with that approach. At the beginning, e.g. Fig. 3a, only a few reflected rays are effectively converging in synchronicity along the cuspidal caustic. After some time the process of focusing becomes more efficient, as more and more rays are converging onto the caustic path. One should emphasise that on Figs. 3 and 4 we have only plotted one single ray over two rays, in order to obtain more realistic and readible results. Moreover, we do start plotting bunch of 50 rays, and then further decreases this number in the following shots to 25, 20 and ultimately 10 rays (see captions for illustrations for further details). For the very last bunch of 10 rays (Fig. 4h), between rays 1 and 10, the concentration of rays simply becomes huge, numerous rays converging at the same time over and over at the locus of the cuspidal feature around D. A composite drawing of the individual results collected onto Figs. 3 and 4 is finally plotted in Fig. 5, showing very neatly the spatial shape of the cuspidal caustic over the quarter cylindrical shell. By symmetry consideration, extension to the full half-cylindrical shell could be retrieved accordingly. A direct and straightforward computation of the focusing coefficient

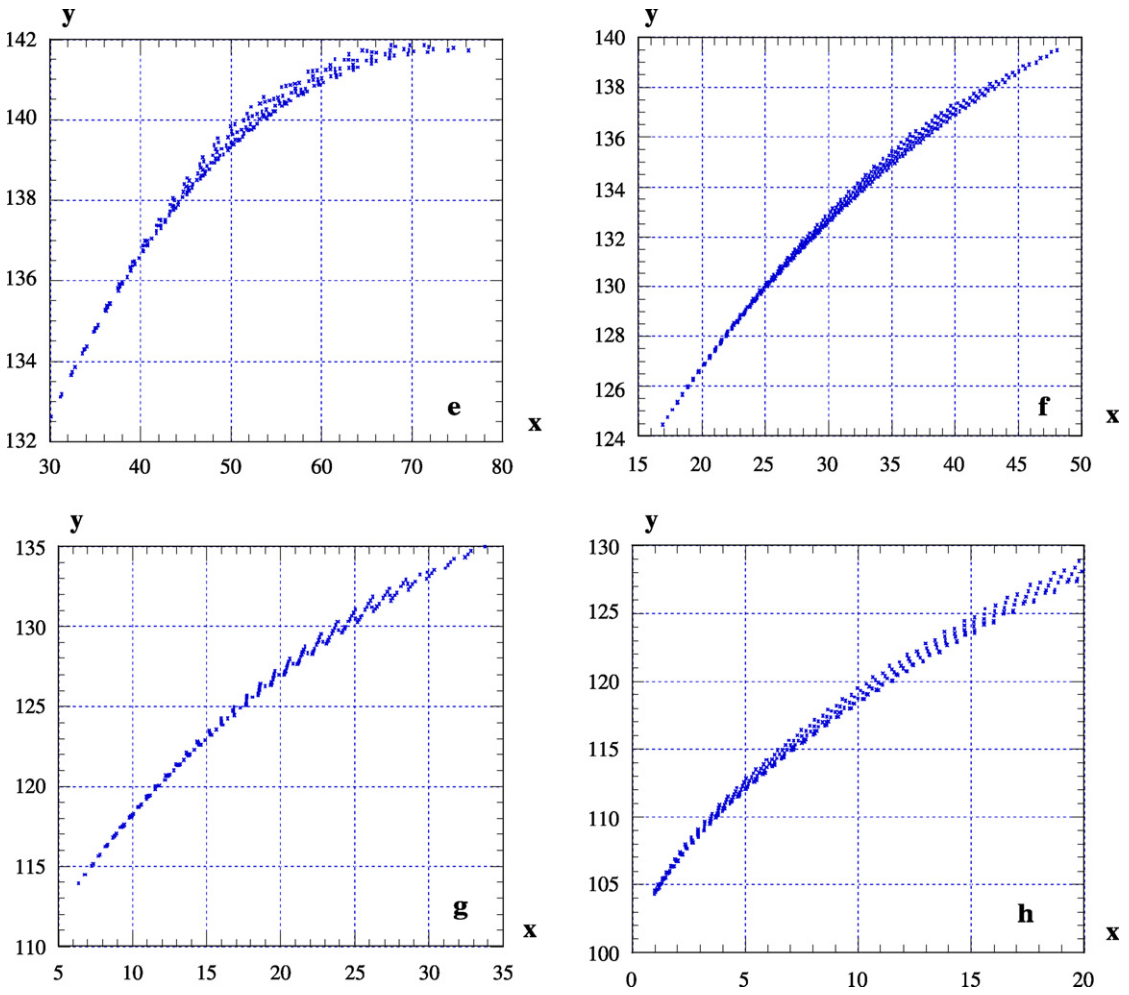

Fig. 4. Results of a ray tracing algorithm showing rays arrivals around the caustic feature. The tracing is done on the 4 various pictures by plotting the progression of only one single ray over two with the following parameters: (e) rays order from 31 to 50; (f) rays order from 21 to 30; (g) rays order from 11 to 20; (h) rays order from 1 to 10.

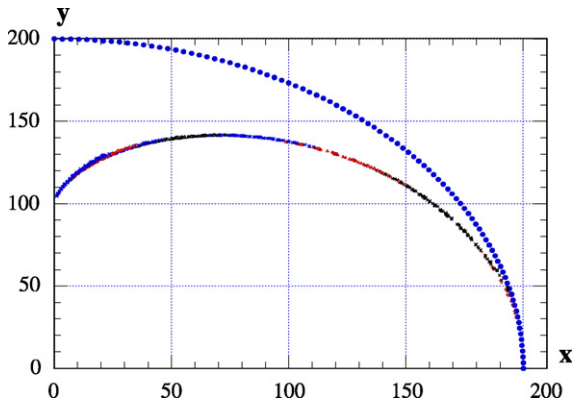

Fig. 5. Composite picture of the two previous drawings showing the full structure of the cuspidal caustic. One can notice the very high concentration of the synchronised reflected waves along the singular feature (point D on Fig. 2, or ray order 0 in the above ray tracing simulations) which correspond to the cusp of the caustic. In such location, the focusing effect is the strongest, the focusing coefficient theoretically diverging to infinity. Obviously, diffraction effects and blurring due to the finite size of the acoustic wavelength (here in the range of 85 mm) limit this divergence to a finite level (as shown in Fig. 7).

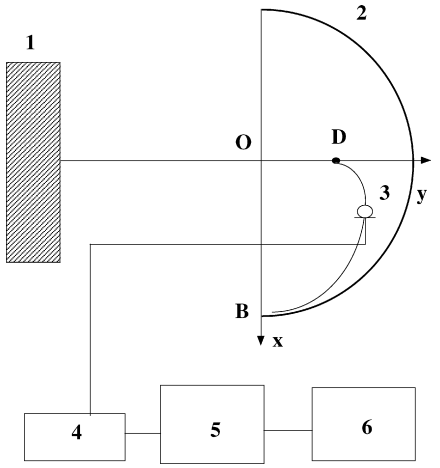

Fig. 6. Schematic diagram of the experimental set-up, showing the main elements: 1—HSS parametric projector; 2—half-cylindrical reflector with a 300 mm radius; 3—audio microphone, type miniature electret; 4—audio amplifier; 5—analog filtering unit; 6—digital oscilloscope and further processing onto a computer.

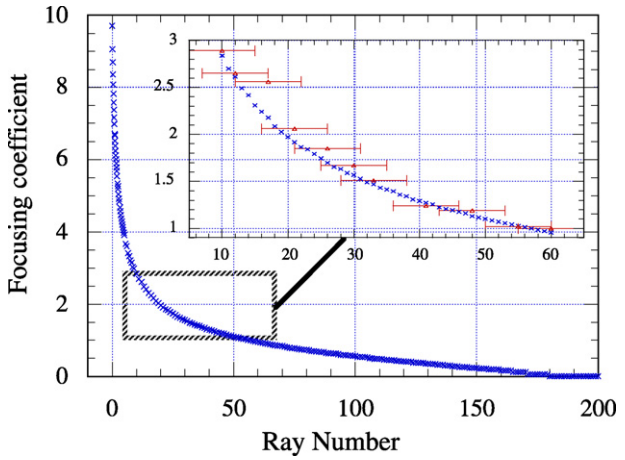

Fig. 7. Computation of the theoretical focusing coefficient from a ray tracing algorithm, and comparisons with experimental data (with horizontal error bars in the insert of the figure). The width of the error bars is an estimation for the spatial incertitude in the positioning of the audio microphone. There is a diffraction theoretical limit which is around a quarter of wavelength, i.e. in the range of 20 mm at 4 kHz, that is approximately the width of the error bars.

is then defined. By knowing the spatial distance between two consecutive incident rays (the so-called ray tube area when dealing with a 3D problem), at initial time (i.e. along the horizontal axis OB of Fig. 2), one defines the measure of their metric distance after appropriate synchronised propagation nearby the caustic (i.e. in its closest vicinity). The ratio between the two metric distances (i.e. the ratio of their ray tube areas) directly provides the focusing coefficient for two consecutive rays. Such quantity is plotted in Fig. 7. It should be noted that the focusing effect do not exist over the full caustic curve. It starts only when the focusing coefficient is larger than one, here approximately at ray #60. Consequently, above that limit, some "defocusing" effect exist, as is already clear from Fig. 3. In fact, on Fig. 3a, one can notice that no pair of rays do exist onto the caustic before $30\Delta t$ along axis y (i.e. the direction of propagation), which in turn explains why the focusing coefficient should tend to zero for the very first rays, as it is documented in Fig. 7. Another, much simplier method to evaluate the focusing coefficient has been used as well. It consists in evaluating the density of tangent reflected waves onto the caustic itself, seen as an envelope curve. The obtained numbers are very similar, even if this second approach somehow is less rigourous, because synchronicity is absent in the reasoning. At the cuspidal feature (location D on Fig. 2), when 200 rays are taken into account, both simulations provide a coefficient of focalisation around 10. This result is obviously linked to the spatial density of the rays, a clear

singularity physically being present around location D. By increasing the number of rays, from 200, to 2000, and then to 20 000, we have seen that the focusing coefficient further increases, having a dependence versus the number of rays which is function of its square root, i.e. it is multiplied by 10 when the total number of rays is augmented by a 100 ratio. This trend was already explained in a 30 years old publication by S.M. Candel [35], and it is related to the Jacobian of the ray transformation along the cuspidal caustic.

4. Comparison with preliminary experimental data in the audio range

The basic aim of the preliminary experimental work, was to ascertain some of the following questions: (1) Are we able to spatially recover the shape of the cuspidal caustic in the audio range? (2) Do we observe the two spatial areas of focusing and defocusing (i.e. having the focusing coefficient in one case larger than one, and otherwise smaller)? (3) Can we retrieve a focusing coefficient close to the one computed during the numerical simulations? (4) What are the spatial limitations drawn on the caustic localisation due to diffraction effects (related to the size of the audio microphone and ancillary diffraction effects) and due to the finite wavelength of the used acoustical wave (here at 4 kHz, that is a theoretical $\lambda/4$ resolution around 20 mm)?

As outlined in the abstract, we have used a commercially parametric projector during the experiments (Fig. 6 provides a schematic diagram of the experimental set-up). This device is manufactured in the USA by the American Technology Corporation, located in San Diego (California). It works at 40 kHz, producing an ultrasonic field at 3 m having a 120 dB level, while the nonlinearly demodulated field at 4 kHz is only 70 dB, at the same distance. The aperture of the audio demodulated field at 4 kHz is around 10 angular degrees at -6 dB. Accordingly, the demodulated wavefield is highly directive (at least when compared to traditional audio sources such as standard loudspeakers), and consequently, the wavefronts are almost planar, enabling to utilise the above analytical and numerical approach, as described in the two previous sections. As noted above, the ultrasonic field is very high, being 100 to 1000 times larger than the demodulated audio field. Consequently, great care should be taken during experiments in order to avoid flaws and errors. An efficient analogic band pass (or low pass) filter unit should be used in order to mostly eliminate the ultrasonic field component through the acquiring electronics. Other precautions should be taken for being confident with the obtained data, for instance to avoid artefacts due to the radiation pressure effect which is always present and very strong. We have here only acquired preliminary data in a manual configuration. Precise positioning of the audio microphone over the caustic region was controlled by pointing a small He–Ne laser. In order to obtain precisely the experimental focusing coefficient, we did proceed as follow. Very short bursts having one single temporal period at 4 kHz were used. Parametric arrays are attractive because such causal extremely short bursts (or wavepackets) are easily obtained. Next, we observe directly on the digital oscilloscope two distinct wave packets, one corresponding to the incident wave (showing up first onto the waveform), and then a second delayed wavepacket related to the reflected synchronised waves arriving at the caustic location (examples of similar waveforms are given in other papers of our group, for different applications [36–38]). A simple ratio between the peak to peak amplitudes of these two wave packets directly yields the focusing coefficient. The raw data obtained with this procedure are gathered in the Table, and they are drawn as an insert zoom plot within Fig. 7. We have restricted ourselves to areas of the caustic demonstrating focusing effect (i.e. having a focusing coefficient larger than 1). We have also tried to avoid being too close to the inner surface of the half-cylindrical reflector, because we have observed a creeping wave (or gallery echoe type wave) progressing along that surface, strongly disturbing the direct amplitude measurements of the reflected waves when the audio microphone is mounted nearby the reflector.

These measurements enable to answer most of the above questions. (1) We do have clearly recovered the spatial shape of the cuspidal caustic. At the same time, and answering part of question (4), the spatial resolution of the path and locus of the caustic is truly limited by diffraction effects, as given by the standard $\lambda/4$ Rayleigh diffraction criterion (see further discussion on this topic below). (2) Focusing and "defocusing" spatial areas do really exist, as shown on the raw data of the Table 1 and as seen in the insert of Fig. 7. We have only documented experimental data corresponding to true focusing effect (focusing coefficient larger than one), but we have observed as well defocusing in other areas of the caustic. The boundary in terms of ray order is correctly retrieved, in the range of ray order #60 (as seen on Fig. 7). (3) The focusing coefficient is correctly recovered, as it is clearly visible on Fig. 7. We do not measure such parameter above 3, but this result is certainly related to spatial resolution and wavelength size restriction. As it was explained in the previous section, numerical simulations do indicate that there exists a numerical singularity at the cusp of the caustic (point D on Fig. 2). This is a physical singularity, where the density of reflected waves

Table 1
Raw experimental data used in the insert of Fig. 7.

Focusing coefficient	Ray order
2.89	10 ± 5
2.63	12 ± 5
2.56	17 ± 5
2.06	21 ± 5
1.85	26 ± 5
1.67	30 ± 5
1.51	33 ± 5
1.24	41 ± 5
1.19	48 ± 5
1.03	55 ± 5
1.00	60 ± 5

increases strongly and possibly diverges. With a very fine mesh during the spatial and temporal finite discretisation (we used 200, 2000 and 20 000 discrete rays and temporal steps), it was numerically possible to obtain very large focusing coefficient, respectively in the range of 10, 30 and 100. Evidently, we are physically limited by the size of the detecting audio microphone and to related diffraction effects around it, and at the same time by the Rayleigh criterion for spatial resolution (here at 4 kHz, $\lambda/4$ is around 20 mm). Accordingly, the cuspidal caustic, instead of being a very well defined curve (as computed onto Figs. 3, 4 and 5), is in fact blurred out by diffraction effects, which defines a band having at 4 kHz, somehow a 20 mm width. Complementary experimental results did clearly demonstrate that point. Consequently, because of this blurring effect, we do not get access during experimental work to precise locations over the caustic better than ± 10 mm, or say in other words at better than 5 or 6 ray orders (the cylinder radius which comprises 200 different rays is approximately 300 mm, that is two consecutive rays are distant by 1.5 mm, or the blurring 20 mm width is above 12 rays). In the insert of Fig. 7, such spatial uncertainty has been plotted with a ± 5 rays error width. This uncertainty explains very clearly that a physical limit should definitely exist on the focusing coefficient, due to diffraction effects. The answer to question (4) is also self-contained in the above explanations.

5. Conclusion and perspectives

The motivation in starting this work came from reflections we had on some practical uses of nonlinear acoustics parametric arrays in the audio range over the 200 Hz–10 kHz bandwidth. Because parametric projectors enable to produce highly directive acoustical plane waves at low frequencies, numerous classical problems of physical acoustics can be revisited in the audio range. They were previously studied in water-tank configurations using ultrasonic waves (in the range of MHz frequencies), or sometimes directly in air at lower ultrasonic frequencies (between 40 and 300 kHz). Here, the main interest lies in directly using much lower frequencies for which other phenomena are occurring nearby boundary layers describing the viscous and thermal damping processes. The thickness of the boundary layers is proportional to the inverse of the square root of the frequency, and consequently, the thickness of the boundary layers (viscous and thermal) which is very small at high frequencies becomes larger when decreasing frequency (at 40 kHz the viscous skin depth is around 10 μm in air, while it is 0.1 mm at 400 Hz). Accordingly, new effects are present when decreasing frequency. Other classical configurations have also been studied with parametric arrays.

We have demonstrated in the present work some significant results for the configuration of focusing onto an half-cylindrical reflector. Strong focusing effects in air occur only nearby the cuspidal feature (around location D in Fig. 2). Numerical simulations based on a ray tracing algorithm enable one to study very precisely the structure of the cuspidal caustic, and the focusing process. Comparison with preliminary experimental data obtained in the audio range in air was adequate. It has been showing that instead of a very fine caustic curve, one gain access to a blurred spatial band whose thickness is related to the standard Rayleigh criterion for diffraction.

References

[1] A.G. Every, Formation of phonon-focusing caustics in crystals, Phys. Rev. B 34 (1986) 2852–2862.

[2] A.L. Shuvalov, A.G. Every, Curvature of acoustic slowness surface of anisotropic solids near symmetry axes, Phys. Rev. B 53 (1996) 14906–14916.
[3] S.I. Tamura, M. Yagi, Finite-wavelength on the ballistic propagation of surface acoustic axes, Phys. Rev. B 49 (1994) 17378–17384.
[4] K.Y. Kim, W. Sachse, A.G. Every, Focusing of acoustic energy at the conical point in zinc, Phys. Rev. Lett. 70 (1993) 3443–3446.
[5] F.S.R. Zhang, S.Y. Lu, SAW focusing by circular-arc interdigital transducers on YZ-$LiNbO_3$, Ultrason. Ferroelectr. Freq. Control 36 (1989) 178–184.
[6] S.M. Flatté, G. Rovner, Calculations of internal-wave-induced fluctuations in ocean-acoustic propagation, J. Acoust. Soc. Am. 108 (2000) 526–534.
[7] J.A. Colosi, E.K. Scheer, S.M. Flatté, et al., Comparisons of measured and predicted acoustic fluctuations for a 3250-km propagation experiment in the eastern north pacific ocean, J. Acoust. Soc. Am. 105 (1999) 3202–3218.
[8] J.A. Simmon, S.M. Flatté, et al., Near-caustic behavior in a 270-km acoustical experiment, J. Acoust. Soc. Am. 105 (1999) 3231–3244.
[9] F.J. Beron-Vera, M.G. Brown, J.A. Colosi, et al., Ray dynamics in a long-range acoustic propagation experiment, J. Acoust. Soc. Am. 114 (2003) 1226–1242.
[10] T. Ishihara, L.B. Felsen, Hybrid(ray)-(parabolic-equation) analysis of propagation in ocean acoustic guiding environments, J. Acoust. Soc. Am. 83 (1988) 950–960.
[11] R. Marchiano, J.L. Thomas, F. Coulouvrat, Experimental simulation of supersonic superboom in a water tank: Nonlinear focusing of weak shock waves at a fold caustic, Phys. Rev. Lett. 91 (2003) 184301.
[12] F. Coulouvrat, Focusing of weak acoustic shock waves at a caustic cusp, Wave Motion 32 (2000) 233–245.
[13] B.E. McDonald, W.A. Kuperman, Time domain formulation for pulse propagation including nonlinear behavior at a caustic, J. Acoust. Soc. Am. 81 (1987) 1406–1417.
[14] P.L. Rendon, F. Coulouvrat, Reflection of caustics and focused sonic booms, Wave Motion 42 (2005) 211–225.
[15] P. Blanc-Benon, B. Lipkens, L. Dallois, M.F. Hamilton, D.T. Blackstock, Propagation of finite amplitude sound through turbulence: Modeling with geometrical acoustics and the parabolic approximation, J. Acoust. Soc. Am. 111 (2002) 487–498.
[16] P. Blanc-Benon, D. Juvé, V.E. Ostashev, On the appearance of caustics for plane sound-wave propagation in moving random media, Waves Rand. Complex Media 5 (1995) 183–199.
[17] M.M. Boone, E.A. Vermaas, A new ray-tracing algorithm for arbitrary inhomogeneous and moving media, including caustics, J. Acoust. Soc. Am. 90 (1991) 2109–2117.
[18] R. Labbé, J.F. Pinton, Propagation of sound through a turbulent vortex, Phys. Rev. Lett. 81 (1998) 1413–1416.
[19] P.S. Theocaris, The axisymetrical buckling parameters in flexed plates as determined by caustics, Eng. Fract. Mech. 52 (1995) 583–597.
[20] V. Aleshin, V. Gusev, V. Tournat, Acoustic modes propagating along the free surface of granular media, J. Acoust. Soc. Am. 121 (2007) 2600–2611.
[21] V. Gusev, V. Aleshin, V. Tournat, Acoustic waves in an elastic channel near the free surface of granular media, Phys. Rev. Lett. 96 (2006) 214301.
[22] X. Jacob, V. Aleshin, V. Tournat, P. Leclaire, W. Lauriks, V. Gusev, Acoustic probing of the jamming transition in an unconsolidated granular medium, Phys. Rev. Lett. 100 (2008) 158003.
[23] W.P. Arnott, P.L. Marston, Unfolding axial caustics of glory scattering with harmonic angular perturbations of toroidal wavefronts, J. Acoust. Soc. Am. 85 (1989) 1427–1440.
[24] M.G. Brown, Space-time surface gravity wave caustics: Structurally stable extreme wave events, Wave Motion 33 (2001) 117–143.
[25] M.G. Brown, The transient wave fields in the vicinity of the elliptic, hyperbolic and parabolic umbilic caustics, J. Acoust. Soc. Am. 79 (1986) 1365–1401.
[26] M.G. Brown, F.D. Tappert, Causality, caustics, and the structure of transient wave fields, J. Acoust. Soc. Am. 80 (1986) 251–255.
[27] M.G. Brown, The transient wave fields in the vicinity of the cuspidal caustics, J. Acoust. Soc. Am. 79 (1986) 1367–1384.
[28] T. Poston, I. Stewart, Catastrophe Theory and Its Applications, Pitman, London, 1976.
[29] I.D. Abrahams, G.A. Kriegsmann, E.L. Reiss, Sound radiation and caustic formation from a point source in a wall shear layer, AIAA J. 32 (1994) 1135.
[30] G.A. Kriegsmann, E.L. Reiss, Acoustic propagation in wall shear flows and the formation of caustics, J. Acoust. Soc. Am. 74 (1983) 1869–1879.
[31] C.J. Chapman, Caustics in cylindrical ducts, Proc. R. Soc. London, Series A 455 (1999) 2529–2548.
[32] G.M. Keith, N. Peake, High-wavenumber acoustic radiation from a thin-walled axisymmetric cylinder, J. Sound Vibration 255 (2002) 129–146.
[33] P.L. Marston, in: W.P. Mason, R.N. Thurston (Eds.), Geometrical and Catastrophe Optics Methods in Acoustical Scattering, in: Physical Acoustics, vol. XXI, Academic Press, New York, 1989.
[34] A.D. Pierce, Acoustics – An Introduction to Its Physical Principles and Applications, 3rd ed., ASA-AIP Edition, New York, 1991, § 8 and 9, pp. 371–507.
[35] S.M. Candel, Numerical solution of conservation equations arising in linear wave theory — Application to aeroacoustics, J. Fluid Mech. 83 (1977) 465–493.
[36] M. Saeid, B. Castagnède, A. Moussatov, V. Tournat, V. Gusev, Application of nonlinearly demodulated acoustic signals for the measurement of the acoustical coefficient of reflection for air saturated porous materials, C. R. Mécanique 332 (2004) 849–858.
[37] B. Castagnède, M. Saeid, A. Moussatov, V. Gusev, V. Tournat, Reflection and transmission at normal incidence onto air-saturated porous materials and direct measurements based on parametric demodulated ultrasonic waves, Ultrasonics 44 (2006) 221–229.
[38] B. Castagnède, A. Moussatov, D. Lafarge, M. Saeid, Metrology of absorption and dispersion of sound absorbing materials on high power ultrasonic non-linearly demodulated waves, Appl. Acoust. 69 (2008) 634–648.